A Novel Multiple-shot Milli-scale Magnetic Robot for Cargo Delivery*

Tamerlan Srymbetov, Arianna Menciassi, *Fellow, IEEE,* and Veronica Iacovacci**, *Member, IEEE*

Abstract—**Magnetic actuation allows distant and safe actuation of small-scale untethered robots. This class of robots is particularly appealing for targeted delivery and on demand release of therapeutic cargo. Most state-of-the-art systems focused so far either on single-shot release or leveraged battery-driven actuation for delivering multiple therapeutic agents' doses. In this work, we propose a novel magnetic milli-scale carrier design that can be distantly navigated and triggered to release 2 or 4 cargo shots, on demand. The carrier features a modular design with a permanent magnet in each compartment. Robot realizations with 1 and 2 compartments are analyzed in this paper. A straightforward control strategy relies on tuning direction and intensity of applied magnetic fields for robot navigation and cargo delivery. Experiments were performed in an aqueous environment to validate carrier locomotion and controlled release capabilities. The prototyped carriers have a parallelepiped shape (12x2x10 mm and 12x6x10 mm for one and two compartments, respectively) and can be wirelessly navigated by an external magnet at a distance larger than 100 mm within 5 mm deviation from the desired trajectory. Upon docking, release can be triggered by modulating the external magnetic field. Quantitative metrics revealed consistent release dosage between prototypes and among different cargo compartments.**

I. INTRODUCTION

Throughout the decades, the concept of a small-scale robot has changed and evolved significantly. At present, small-scale robotics includes a wide class of systems ranging from hundreds of nanometers to few millimeters in size and able to navigate or execute tasks in response to precise control inputs [1]. Small-scale robots are particularly intriguing for biomedical applications in light of their dexterity, hard-to-reach targeting capabilities and wireless controllability. This can be appealing in cargo delivery [2], diagnostics, and targeted therapy applications [3].

At the millimeter scale, untethered robots also have considerable controllability, payload transport capabilities, and sufficient speed to withstand dynamic environments. Various strategies have been proposed in the literature to actively navigate the robots and to trigger task execution: magnetic fields [4], acoustic fields [5], light [6], fluid flow [7], and their combinations [8]. Among them, magnetic fields enable remote actuation at distances between the source and the target that can match body anatomy. Furthermore, magnetic fields are safe as well as able to cross all body tissue with almost no attenuation.

Considering millimeter scale magnetic carriers, one can find numerous examples in the literature where designs based mainly on permanent magnets were proposed for drug delivery in the GI tract [9], in the bloodstream [4] and in other body districts [10] as well as for tissue biopsy [11] [12]. Some works also explore the use of electronics for powering actuators and/or for wireless communication [13].

Despite the wide plethora of solutions proposed to perform controlled release of a therapeutic cargo while leveraging magnetic forces, most of them are intended to release the cargo all at once, i.e., *single-shot* release. These robots exclude applicative scenarios where cargo release in multiple adjacent locations would be desirable or different therapeutic agents should be delivered in a single procedure. For example, delayed sequential co-delivery of drugs during chemotherapy [14] or other treatments [15].

Researchers have proposed untethered milli-scale robots with multiple compartments to controllably release several drug shots but generally employed battery-run electrical components in their designs [16]. To the best of our knowledge, only one recent work proposed a battery-free untethered small-scale robot that can be actively controlled and capable of on-demand discrete cargo release of multiple drugs [17]. Here, researchers employ alternate magnetic fields at high frequency (up to 180 Hz) to deflect a magnetic soft beam. This high-frequency actuation makes the approach hard to scale over larger workspaces.

In this work, we attempt to tackle the aforementioned challenges by proposing a novel externally triggerable magnetic carrier that can deliver multiple cargo doses on demand upon an uncomplicated magnetic actuation, i.e., *multiple-shot* robot (Fig. 1a). The proposed robot has a modular design that allows combination of multiple compartments, each including an internal permanent magnet (IPM) with a radial magnetization. Every compartment has two reservoirs, and an external permanent magnet (EPM) can trigger cargo release at a controlled distance. The use of compartments made of different materials with distinct friction coefficients and with different IPMs magnetization ensures a selective and sequential release-triggering.

The proposed design appears modular and provides the opportunity to select the number of modules, i.e., compartments, depending on the target application scenario. In this direction, multiple-shot robots with one and two compartments were considered in this work, which are later recalled as MSR1 and MSR2, respectively (Figure 1).

All authors are with The BioRobotics Institute, Scuola Superiore Sant'Anna, Pontedera (Pisa), Italy.
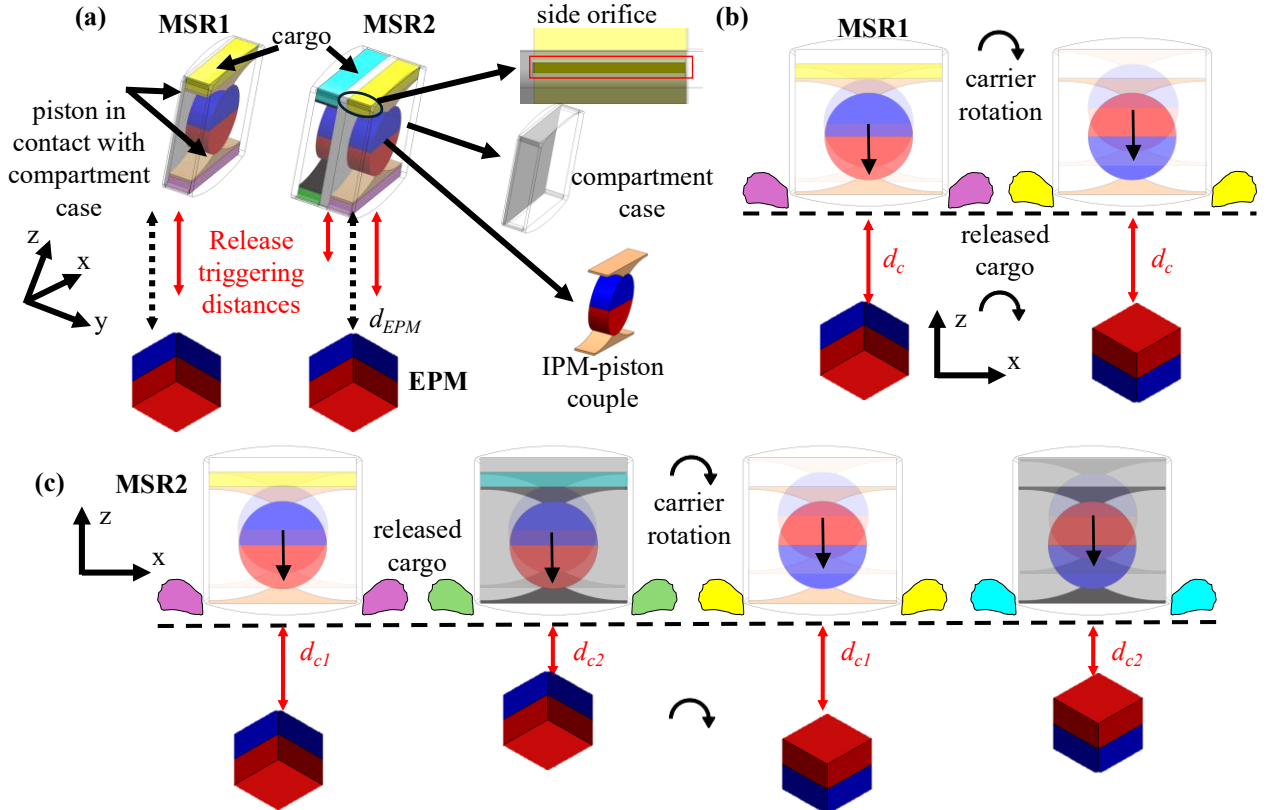
Fig. 1. Proposed multiple-shot robot design. (a) Schematic of the robot with 1 and 2 compartments (MSR1 and MSR2) with detailed representation of the side orifices intended for release and the IPM-piston couple which represents the central element of each compartment and of the release mechanism. In the MSR2 design the two compartment pistons are depicted with different colors to represent the differences in the constitutive materials. (b-c) Schematization of the release sequence of 2 cargo doses (b) and 4 cargo doses (c), upon IPM alignment with and attraction by external permanent magnet (EPM) at critical release-triggering distances. In the image different colors mean different materials for pistons and compartments as well different cargo (purple, yellow, green, and light blue).

The remainder of the paper is organized as follows: Section II describes the methodological steps to study the proposed carrier design, Section III presents major numerical and experimental results, and Section IV provides final considerations on the work.

II. MATERIALS AND METHODS

A. System Overview

A single EPM can be used to control carrier locomotion and cargo release. The use of an EPM allows distant actuation with a larger workspace and the production of magnetic field gradients much higher than what can be produced by conventional electromagnetic systems.

A stable carrier configuration is the loaded one, where each IPM is in the middle of the compartment and all cargo reservoirs are full.

MSR1 design is built around a single disc-shaped radial IPM, which is attached to a double-side piston and has magnet poles aligned with the piston stroke direction. When an EPM approaches, the carrier first aligns to the applied magnetic field (Fig. 1b). Once the EPM approaches a critical distance d_c from the carrier, magnetic attraction overcomes the friction forces holding the IPM and the piston in place, which initiates the cargo release. By changing the EPM orientation through rotation, we can repeat the procedure from the other side, thus resulting in the release of two distinct cargo doses.

Considering a 2 compartments design, namely MSR2, two distinct critical distance values d_{c1} and d_{c2} should be considered at which 1st and 2nd compartments are release-triggered, respectively (Fig. 1c). The sequential release is governed by differences in constitutive materials (piston and compartment case) and IPM magnetization and size among adjacent compartments: this induces a different balance among friction and magnetic force that turns into the possibility to selectively trigger the release of a cargo dose when tuning the applied magnetic force, which depends on the distance to EPM and its orientation.

B. Numerical and Analytical Modelling

In order to realize the proposed robotic design, a thorough modelling is crucial. As the carrier has several stable configurations, we need to formulate the conditions for each of them to be controllably reached. Then, it is needed to find conditions for a controlled release-triggering at distinctly different critical distances. Finally, locomotion modelling verifies if a carrier can be distantly navigated without triggering the release.

1) Modelling of a Loaded Carrier Configuration

Figure 2a illustrates major forces acting on IPMs. Additionally, Fig. 2b displays major parameters to be considered when dimensioning a carrier. Naturally, most dimensions are inter-dependent and should be iterated together during modelling.
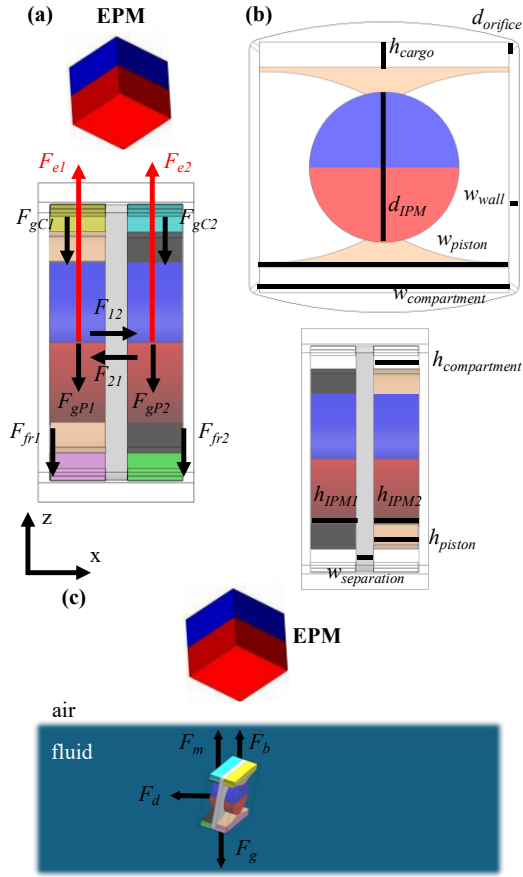
Fig. 2. Proposed magnetic carrier design (a) force-balance analysis during release-triggering and when loaded. (b) As an input to the model, major dimensions of the robot components are illustrated. (c) For the locomotion analysis, a dedicated force-balance analysis was employed. In the figure, different cargo in the reservoirs and non-magnetic materials are stylized with different colors.

When loaded with cargo, the piston should be stable in place. Indeed, the friction force F_{fr} between compartment walls and IPM-piston couples should balance the gravity force F_g (of IPM-piston couple F_{gP} and of cargo F_{gC}) and the magnetic force F_m between IPMs and EPM (F_{e1} and F_{e2}), and among IPMs in MSR2 (F_{12} and F_{21}).

$$|F_m + F_g| < F_{fr}, \tag{1}$$

where $F_{m1} = F_{e1} + F_{21}$, and $F_{g1} = F_{gP1} + F_{gC1}$ for IPM1, and $F_{m2} = F_{e2} + F_{12}$, and $F_{g2} = F_{gP2} + F_{gC2}$ for IPM2.

For MSR1, a worst-case scenario is a vertical carrier orientation, i.e., a gravity acting in -z direction. Here, while neglecting magnetic forces, maximum gravity force values are applied on the piston to move it. Therefore, to keep it in place, press-fitting or interference forces should be considered during assembly [18]. This primarily imposes design conditions on piston height ($h_{piston} > h_{compartment}$) and/or piston width ($w_{piston} > w_{compartment}$) (Fig. 2b). The friction force due to interference-fitting depends on the materials used, i.e., the friction coefficient between the components, and wall thickness w_{wall}, with details given further with equation (4). All these parameters should be iterated to derive feasible prototype designs.

For MSR2, IPMs repel each other (F_{12} and F_{21}), thus causing an increase in friction force and making triggering activation more force-demanding. Therefore, no piston interference is needed to hold the IPM-piston couples in place. Naturally, the repulsion force depends on $w_{separation}$, and if the separation increases, IPMs interaction weakens. Therefore, balancing between carrier size (increase of $w_{separation}$), piston stability (smaller $w_{separation}$), and release-triggering distances (larger $w_{separation}$ means a smaller holding force to overcome) should be pursued.

To note, in this work, we do not use spring elastic elements to hold the IPM when loaded and bring it back when the EPM is distant from a carrier. An assumption was made that the inclusion of these elements would make the system bulkier.

2) Modelling of a Release Activation

When release has to be triggered, the main model output is the critical distance between the EPM and IPM able to produce piston movement. To initiate release, the friction force keeping the IPM in place should be overcome by the applied magnetic force:

$$|F_m + F_g| > F_{fr}, \tag{2}$$

For MSR2, it is important to ensure the selective activation of each compartment. As such, when the first compartment release is activated, the other IPM should remain in the loaded configuration:

$$|F_{m1} + F_{g1}| > F_{fr1} \cap |F_{m2} + F_{g2}| > F_{fr2} \tag{3}$$

At the same time, a critical release-triggering distance of the second compartment should be found using (2). As mentioned, sequential release-triggering is ensured with compartments having IPMs of different strength (Br) and different materials with distinct friction coefficients. If the EPM is approaching with an opposite orientation, the release-triggering sequence is the same.

Since IPMs are considerably close to each other and to the EPM, a Finite Element Method (FEM) tool (COMSOL Multiphysics) was used to compute magnetic forces for the release activation analysis: F_{12}, F_{21}, F_{e1}, and F_{e2}. A stationary study with Magnetic Fields module was run while varying $w_{separation}$, distance to the EPM d_c, IPMs size and grades.

In this analysis, commercially available IPMs and the strongest available EPM were considered. The latter is 60 mm in diameter with a 10 mm hole, 70 mm in height, and N42 grade. Data analysis could then be used to find configurations satisfying (2) and (3).

The selected magnets should not only meet the model specifications, but also allow the production of a miniaturized prototype with reference to a 000-capsule size, which has a maximum diameter of 10 mm. Therefore, ($w_{compartment} + 2\ w_{wall} < 10\ mm$) and ($2\ h_{compartment} + 2\ w_{wall} + w_{separation} < 10\ mm$) have to be satisfied.

MSR1 was designed identically to the first compartment of MSR2 to favor results comparison. We set h_{piston} equal to $h_{compartment}$ as the piston front has a large contact area with the compartment, which increases the interference force. Therefore, we iterated interference in the piston width ($w_{piston} - w_{compartment}$) to have a piston-holding friction force.

The friction force due to piston interference (F_{frInt}) should be just slightly larger than F_g to ensure both stability in the loaded configuration and a relatively small external magnetic attraction force to initiate the release. The friction force can be defined as:
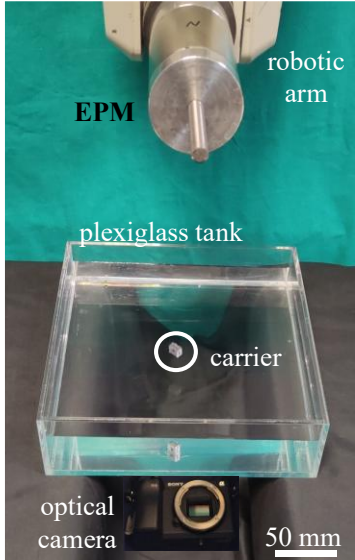
Fig. 3. Testing setup for release-triggering and locomotion experiments.

$$F_{frInt} = \frac{2\,\mu_{fr}\,(w_{piston} - w_{compartment})\,A_{crossP}}{w_{piston} \left[\frac{w_{wall}}{E_{piston}\,(1-v_{piston}^2)} + \frac{w_{wall}}{E_{wall}\,(1-v_{wall}^2)}\right]}, \quad (4)$$

where A_{crossP} is the piston cross-section area in contact with the compartment wall, E and v are the piston Young's modulus and Poisson's ratio, respectively. This explains how, by changing piston and compartment constitutive materials, the friction force can be modulated to activate selective cargo release.

3) Locomotion Modelling

To produce robot locomotion in water, there are three main forces to consider: gravity F_g, buoyancy F_b, drag F_d, and magnetic attraction toward EPM F_m (Fig. 2c). Since IPMs are quite distant from EPM, the magnetic dipole approximation was used to compute the magnetic forces needed to let the robot drag.

Carrier navigation was performed in the floating configuration, so when considering it fully immersed in water. Here, the magnetic attraction force should be strong enough to keep it underwater but also weaker than the gravity force so that a robot does not escape the fluid medium.

In this work, an EPM is navigating a floating carrier along certain trajectories. To achieve the most distant locomotion performance, an EPM must have a magnetization vector perpendicular to the fluid surface, assuming there is enough space for a carrier to rotate, so that IPMs and, hence, the carrier, are aligned with EPM magnetization(Fig. 2c). Given carrier dimensions, IPMs sizes and grades, a quantitative output of the locomotion model would be the range of distances at which the carrier floats d_{float} and can be navigated by an EPM. Outside of this range, the carrier either sinks or escapes the fluid medium toward the EPM. Naturally, a minimum d_{float} value has to be greater than d_{c1} and d_{c2} in order to avoid unwanted release.

C. Materials Selection and Robots Prototyping

Off-the-shelf magnets were analyzed for robot prototyping. The choice was made for the combination of IPMs of similar size, keeping the carrier dimensions within the 000 capsule size standard (26.14x9.97 mm), and allowing distinct release-triggering distances. 3x1 and 2.5x1 mm NdFeB permanent disc-magnets were used as an IPM for MSR1 and as IPM1 for MSR2, and as IPM2 for MSR2, respectively. During modelling, 5 mm was chosen as a minimum distance from an EPM to keep the remote actuation advantages associated with magnetic actuation.

The SLA Formlabs printer was used to fabricate non-magnetic components. The main material properties to consider were static friction coefficient and stiffness, which helps to avoid large deformations and fractures during the actuation. No surface treatments were used to further tune the properties.

D. Testing and Validation Procedures

Figure 3 displays the testing environment. For a distant actuation, a 60x10x70 mm cylindrical N42-grade EPM with a radial magnetization was used. The magnet could be mounted on a dexterous 6DOF robotic arm (Melfa RV-3SB, Mitsubishi). Tests were performed in a transparent plexiglass tank filled with water. Recording of release-triggering and locomotion experiments was ensured by an optical camera. For both designs, 5 realizations were tested.

For the release experiments, the main quantitative output to validate was the release-triggering distances, predicted by the model. The robotic arm controls EPM position with a 1 mm step until a release was triggered, which was registered with a dye release. These values were measured for each robot compartment based on 10 sample statistics. Compartments were filled with a black dye for the qualitative confirmation of each reservoir release-triggering.

In order to assess the release consistency (repeatability among different release events and between different prototypes), we calculated a quantitative image-based release coefficient RC, presented in a previous work [19]:

$$RC = (Area \cdot BGV)/(1000 \cdot MGV) \quad (5)$$

where $Area$ is the total number of pixels in the enclosed area of the released dye, MGV is the mean gray value within this area, and BGV is the mean gray value of a background sample in an image to account for different lighting.

For the locomotion experiments, we could measure a maximum distance from the EPM at which a carrier floats $d_{floatMax}$ and how close a carrier follows a planned trajectory while floating. The former could be numerically predicted and used for model validation. For the latter, an optical camera was used to record from the bottom the carrier motion in response to the EPM movement, as shown in Fig. 3. Then, the *Tracker* software [20] was used to calculate the carrier coordinates during the locomotion, which were then used to calculate the deviation from the planned trajectory ($\Delta_{trajectory}$).

III. RESULTS

A. Numerical Model Results

For locomotion and release-triggering performance, two major quantitative outputs could be obtained, which are critical release-triggering distances d_c and the floating distance range d_{float} (Table I). The predicted d_{float} is high enough to be
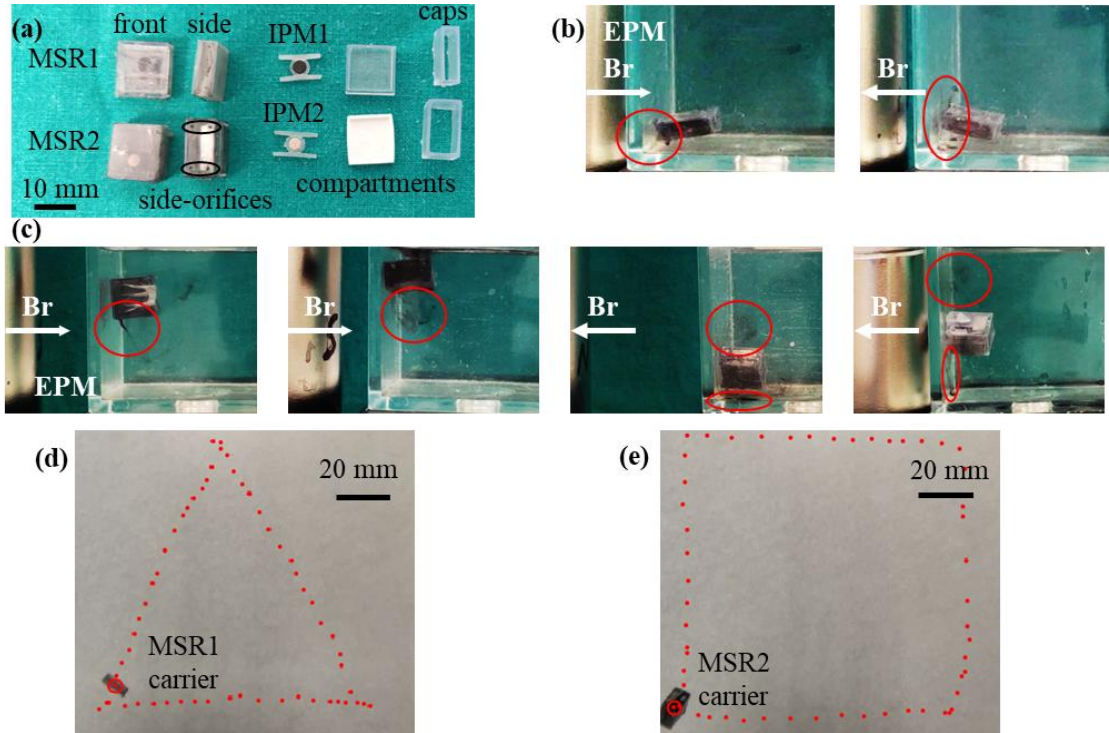
Fig. 4. Experimental results: (a) realized prototypes of both robot designs, sequential cargo release performance of (b) 1 and (c) 2 compartments robots. Here, Br refers to EPM remanent flux density. For the locomotion tests, a sample trajectory following along are shown for (d) MSR1 and (e) MSR2.

sufficient in the vast majority of applications and is also given in a sufficiently large range, allowing a wide safety margin. In these ranges, a minimum refers to a distance at which a carrier escapes a fluid medium, while the upper bound refers to a carrier sinking. If compared to release-triggering distance, there is a safety margin of at least 50 mm within which the carrier can be navigated without release-triggering.

TABLE I
MAIN NUMERICAL RESULTS AND SELECTED PARAMETERS FOR THE PROTOTYPES' FABRICATION

Components	MSR1	MSR2	
		Compartment 1	Compartment 2
IPM size* [mm]	3x1	3x1	2.5x1
B_r [Tesla]	1.4	1.4	1.32
d_c [mm]	39	33	20
d_{float} [mm]	99-146	84.5-148	
μ_{fr}	0.52	0.52	1
V_{cargo} [μl]	2 x 11	4 x 11	
Dimensions [mm]	12 x 2 x 10	12 x 6 x 10	

* d_{IPM} x h_{IPM}

The final prototypes can be found in Fig. 4a. For MSR2, a $w_{separation}$ of 2 mm was found sufficient to keep adequate repulsive magnetic forces between the selected IPMs and to guarantee stability in the loaded configuration. To fabricate non-magnetic components, Biomed Clear and Rigid 10k resins were used, which have distinct static friction coefficients of 0.52 and 1. As a result, for MSR2, it was possible to achieve distinct d_{c1} and d_{c2} listed in Table II. During assembly, the carriers are sealed using Parafilm (Sigma-Aldrich) in order to reduce cargo leakage.

B. Release Performance

For both designs, experimental d_c features some discrepancies with respect to numerical predictions. Importantly, d_c and d_{c1} for MSR1 and MSR2 are relatively close to the predicted values, while d_{c2} is significantly smaller than the predicted one. Such behavior is even more beneficial for the proposed design since we get considerably different critical release-triggering distances for the two compartments, thus favoring selective release activation success. A smaller release-triggering distance can be explained by print and assembly imperfections, which cause an increase in the friction force. Also, a more complex interaction between IPM1 and IPM2 than what was predicted by COMSOL might occur, especially after the IPM1 movement.

Release performance-related results are given in Fig. 4. Here, Fig. 4b-c recorded images demonstrate the sequential release capabilities of the prototypes across both designs. The measured data are summarized in Table II.

In Table II, release coefficient RC values are calculated based on 5 samples per design. This qualitative analysis revealed that there is a high repeatability between different shots released by the same carrier and when varying the carrier prototype. A relatively close relation among separate compartments release shots as well as between the proposed designs is evident. During the experiments, sometimes the carrier was not well aligned with EPM and could not be self-aligned due to high friction force. In these cases, a cargo release could not be triggered. However, small side movements of the EPM within 10 mm would realign the carrier and trigger the release ensuring high success rate in release triggering.

TABLE II
Main Experimental Results

Components	MSR1	MSR2	
		Compartment 1	Compartment 2
d_c [mm]	31.9±5.4	32.7±3.5	12.3±2.4
$d_{floatMax}$ [mm]	175±15	184±11	
RC	6.9±3.1	6.1±2.8	
Δ_{square} [mm]	4.1±1.1	4.2±1.7	
$\Delta_{triangle}$ [mm]	3.6±1.6	4.5±2.6	

C. Locomotion Performance

Experimental $d_{floatMax}$ proved larger than the one predicted by the model. This can be explained by some air pockets present inside the carrier, which increases the lifting buoyancy force.

Robots tracking during navigation along square and triangular trajectories proved a trajectory deviation of about half body length (Fig. 4d-e). Both trajectories could be followed with approximately the same deviation for both MSR1 and MSR2. During experiments, EPM was placed at 120 mm from a floating carrier and moved with 10 mm/s, which is the default speed for the used robotic arm. The triangle and square trajectory sides are equal to 10 body lengths.

IV. Discussions and Conclusions

Presented in this work, the possibility of discrete and distinct cargo or drug dosing makes this robot applicable to numerous applications, where delayed or sequential cargo delivery increases the therapeutic effect [14], [15]. Our proposed design is unique in this field as a milli-scale magnetic robot that can be actively navigated, controlled without on-board powering sources.

For future work, release performance should be enhanced with an orifice membrane to avoid undesired leakage. In this work, a water dye highlighted sealing issues of the realized prototypes. Therefore, a flexible release-triggered orifice membrane is needed to ensure no cargo leakage. Furthermore, different distinct cargos will be interesting, e.g., particle dispersions. Also, surface treatments or different materials will be essential to explore more distinct materials for prototyping in terms of friction. Lastly, further miniaturization and general scalability will be important to study. Experimentally, a more complex working environment will have to be considered by including compliant walls, constrained workspace, and the need for position feedback, e.g., ultrasound [21], in a closed-loop control scenario.

V. References

[1] V. Iacovacci, E. Diller, D. Ahmed and A. Menciassi, "Medical Microrobots," *Annual Review of Biomedical Engineering,* vol. 26, pp. 561-591, 2024.

[2] M. Kim, J. D. Nicholas, J. Puigmarti-Luis, B. J. Nelson and S. Pane, "Targeted Drug Delivery: From Chemistry to Robotics at Small Scales," *Annual Reviews,* vol. 8, 2025.

[3] J. Li, B. E.-F. De Avila, W. Gao, L. Zhang and J. Wang, "Micro/nanorobots for biomedicine: Delivery, surgery, sensing, and detoxification," *Science Robotics,* vol. 2, no. 4, 2017.

[4] K. Choi, G. Jang, S. Jeon and J. Nam, "Capsule-type magnetic Microrobot actuated by an external magnetic field for selective drug delivery in human blood vessels.," *Transactions on Magnetics,* vol. 50, no. 11, pp. 1-4, 2014.

[5] J. J. Kwan, R. Myers, C. M. Coviello, S. M. Graham, A. R. Shah, E. Stride, R. C. Carlisle and C. C. Coussios, "Ultrasound-Propelled Nanocups for Drug Delivery," *Small,* vol. 11, no. 39, pp. 5305-14, 2015.

[6] M. Xuan, Z. Wu, J. Shao, L. Dai, T. Si and Q. He, "Near Infrared Light-Powered Janus Mesoporous Silica Nanoparticle Motors," *Journal of the American Chemical Society,* vol. 138, no. 20, 2016.

[7] D. Ahmed, X. Mao, B. K. Juluri and T. J. Huang, "A fast microfluidic mixer based on acoustically driven sidewall-trapped microbubbles," *Microfluidics and Nanofluidics,* vol. 7, pp. 727-731, 2009.

[8] D. Ahmed, T. Baasch, N. Blondel, N. Laubli, J. Dual and B. Nelson, "Neutrophil-inspired propulsion in a combined acoustic and magnetic field," *Nature Communications,* vol. 8, 2017.

[9] M. Simi, P. Valdastri, C. Quaglia, A. Menciassi and P. Dario, "Design, Fabrication, and Testing of a Capsule With Hybrid Locomotion for Gastrointestinal Tract Exploration," *IEEE/ASME Transactions on Mechatronics,* vol. 15, no. 2, 2010.

[10] V. Iacovacci, G. Lucarini, L. Ricotti, P. Dario, P. E. Dupont and A. Menciassi, "Untethered magnetic millirobot for targeted drug delivery," *Biomed Microdevices,* vol. 17, no. 63, 2015.

[11] Y. Xiang, R. Liu, Z. Wei, X. Wang, W. Kang and M. Wang, "MINRob: A Large Force-Outputting Miniature Robot Based on a Triple-Magnet System," *IEEE Transactions on Robotics,* vol. 40, pp. 3127 - 3145, 2024.

[12] C. M. Hoang, V. H. Le, J. Kim, E. Choi, B. Kang, J.-O. Park and C.-S. Kim, "Untethered Robotic Motion and Rotating Blade Mechanism for Actively Locomotive Biopsy Capsule Endoscope," *IEEE Access,* vol. 7, 2019.

[13] O. Alonso, A. Dieguez, S. Schostek and M. O. Schurr, "A System-on-Chip Solution for a Low Power Active Capsule Endoscope with Therapeutic Capabilities for Clip Application in the Gastrointestinal Tract," *Journal of Medical Robotics Research,* vol. 2, no. 4, 2017.

[14] Z. Zhou, M. Jafari, V. Sriram, J. Kim, J.-Y. Lee, S. J. Ruiz-Torres and S. E. Waltz, "Delayed Sequential Co-Delivery of Gefitinib and Doxorubicin for Targeted Combination Chemotherapy," *Molecular Pharmaceutics,* vol. 14, no. 12, pp. 4551-4559, 2017.

[15] A. Gazzaniga, S. Moutaharrik, I. Filippin, A. Foppoli, L. Palugan, A. Maroni and M. Cerea, "Time-Based Formulation Strategies for Colon Drug Delivery," *Pharmaceutics,* vol. 14, 2022.

[16] Z. Li, T. Wei, Y. Z. Liu, C. Du, C. Shi and C. Hu, "Rotating Multibarreled Capsule Robot for Multiple Biopsies and On-Demand Drug Delivery," *IEEE/ASME Transactions on Mechatronics,* 2025.

[17] Z. Yang, C. Xu, J. X. Lee and G. Z. Lum, "Magnetic Miniature Soft Robot with Reprogrammable Drug-Dispensing Functionalities: Toward Advanced Targeted Combination Therapy," *Advanced Materials,* 2024.

[18] T. H. Brown Jr., "Chapter 3: Advanced Loadings," in *Mark's Calculations for Machine Design*, McGRAW-HILL, 2005, pp. 127-152.

[19] T. Srymbetov, G. De Angelis, Menciassi A and V. Iacovacci, "Millimeter-scale Magnetic Carrier for On-demand Delivery of Magnetic and Non-magnetic Microparticles Suspensions," in *10th IEEE RAS/EMBS International Conference for Biomedical Robotics and Biomechatronics (BioRob)*, Heidelberg, 2024.

[20] D. Brown, "Video Modeling: Combining Dynamic Model Simulations with Traditional Video Analysis," 2008. [Online]. Available: https://opensourcephysics.github.io/tracker-website/download/video_modeling.pdf.

[21] S. Pane, G. Faoro, E. Sinibaldi, V. Iacovacci and A. Menciassi, "Ultrasound Acoustic Phase Analysis Enables Robotic Visual-Servoing of Magnetic Microrobots," *IEEE Transactions on Robotics,* vol. 38, no. 3, pp. 1571 - 1582, 2022.